Research Article Vol. 37, No. 11 / November 2020 / Journal of the Optical Society of America B A69

Journal of the Optical Society of America B

OPTICAL PHYSICS

Coexistence of bright and dark cavity solitons in microresonators with zero, normal, and anomalous group-velocity dispersion: a switching wave approach

JIMMI HERVÉ TALLA MBÉ[1,*] AND YANNE K. CHEMBO[2]

[1]Laboratory of Condensed Matter, Electronics and Signal Processing, Department of Physics, University of Dschang, P.O. Box 67, Dschang, Cameroon

[2]Department of Electrical and Computer Engineering, and Institute for Research in Electronics and Applied Physics, University of Maryland, College Park, Maryland 20742, USA

*Corresponding author: jhtallam@yahoo.fr

Received 30 April 2020; revised 18 June 2020; accepted 18 June 2020; posted 19 June 2020 (Doc. ID 396610); published 16 July 2020

We propose a theoretical study to analyze how both dark and bright Kerr solitons can be generated in whispering-gallery mode resonators with various regimes of the group-velocity dispersion, namely normal, anomalous, and null. The coexistence of these solitonic structures in each regime is shown to appear around a critical value of the laser pump. We also evidence that these solitons build up owing to a mechanism related to oscillation locking of switching waves, which connect the upper and the lower homogenous steady states.

https://doi.org/10.1364/JOSAB.396610

1. INTRODUCTION

The generation of optical frequency combs using whispering-gallery mode (WGM) resonators with Kerr nonlinearity has been intensely studied in recent years. These Kerr frequency combs are the spectral representation of nonlinear dissipative patterns traveling inside the resonator [1,2]. Indeed, Kerr frequency combs are generated through a cascade of nondegenerate photonic interactions known as four-wave mixing, where two photons interact via Kerr nonlinearity to yield two output photons with different frequencies. From the mathematical point of view, the topic of Kerr combs is an extension of a previous body work dealing with Kerr-nonlinear cavities pumped with a continuous-wave laser (see [3,4] and review article [5]).

The study of Kerr optical frequency combs has demonstrated a plethora of novel solitonic effects, with immediate applications that include precision measurement and optical signal processing [2,6–21]. However, its scope has been widened to incorporate atomic/molecular clock and spectroscopy [22–24], telecommunication engineering [25–27], astrophysics [28], biology [29], and integrated photonics [30–32].

Dispersion is required for a Kerr comb to be generated [1,2,33]. From this requirement, one can foreshadow the central role that it plays, and several studies have focused on investigating its various effects. In general, the most prevalent dispersion term corresponds to second-order dispersion, also referred to as group-velocity dispersion (GVD). Bright solitons are usually obtained with negative GVD (anomalous regime) [15,34,35], while dark solitons are favored when the GVD is positive (normal regime) [15,36–38]. It is important to note that the dispersion of a resonator can to some extent be engineered to yield a dispersion profile closely corresponding to arbitrary configurations [39–45].

Recent research in the normal dispersion regime has highlighted a mechanism leading to the emergence of dark and bright solitons via switching waves connecting the homogenous steady-state solutions that underlay the architecture of these solitons [36,37]. More precisely, these switching waves are traveling front solutions connecting the upper and lower homogenous steady-state solutions [36–38,46,47]. Dark solitons originate from the oscillation interlocking of these switching waves around the lower steady state, whereas bright solitons are a consequence of the same process around the upper steady state. The coexistence of bright and dark solitons was also demonstrated with normal GVD and attributed to a joint contribution of the third-order dispersion (TOD) and high detuning [38]. Moreover, the coexistence of both bright and dark solitons was also demonstrated in the case of zero GVD [48]. However, the origin of this coexistence was not investigated. Furthermore, and to best of our knowledge, such coexistence has not yet been considered in the case of resonators featuring anomalous GVD.

In this paper, we study the mechanism that is at the origin of the coexistence of bright and dark solitons in Kerr-nonlinear WGM resonators. The paper is organized as follows. In Section 2, we briefly present the model, while Section 3 highlights the switching wave phenomenology that allows for the coexistence of solitons in the zero-GVD regime. In Section 4, we use the same method to evidence the coexistence of the solitonic waveforms in both the normal and anomalous GVD regimes. The last section concludes the article.

2. THE MODEL

The spatiotemporal dynamics of intracavity laser fields in WGM resonators is described with high precision by the mean-field Lugiato–Lefever equation (LLE) [3]. In a dimensionless form, the generalized LLE can be explicitly written as

$$\frac{\partial \psi}{\partial t} = F - (1 + i\alpha)\psi + i|\psi|^2\psi + i\sum_{n=2}^{n_{\max}} i^n \frac{b_n}{n!}\frac{\partial^n \psi}{\partial \theta^n}, \quad (1)$$

where $\psi(\theta, t)$ represents the complex slowly varying envelope of the total intracavity field, which is related to the intracavity power in watts by $|E|^2 = [\hbar\omega_{\text{las}}/2g_0\tau_{\text{ph}}T_{\text{FSR}}]|\psi|^2$, with $T_{\text{FSR}} = 2\pi/\Omega_{\text{FSR}}$ being the intracavity round-trip time, whereas Ω_{FSR} is the angular free-spectral range (FSR) of the resonator. The parameter g_0 is characteristic of the Kerr response and proportional to the nonlinear coefficient n_2 of the refraction index. The dimensionless time t in Eq. (1) is obtained by rescaling the time with twice the photon lifetime, following $2\tau_{\text{ph}} = 2/\Delta\omega_{\text{tot}}$, where $\Delta\omega_{\text{tot}}$ is the total linewidth of the pumped resonance. The variable $\theta \in [-\pi, \pi]$ stands for the azimuthal angle along the circumference of the resonator, and F is the dimensionless pump field of the resonator. The parameter $\alpha = -2\sigma/\Delta\omega_{\text{tot}}$ is the dimensionless frequency detuning parameter with $\sigma = \omega_{\text{las}} - \omega_{\text{res}}$ (frequency detuning) being the difference between the angular frequencies of the pumping laser (ω_{las}) and the cold-cavity resonance (ω_{res}). The nth-order dispersion parameters b_n ($2 \le n \le n_{\max}$) can be expressed as

$$b_n = 2v_g\tau_{\text{ph}}\beta_n\Omega_{\text{FSR}}^n. \quad (2)$$

A contribution of $b_{n\ge 2}$ expresses the deviation of the resonance frequencies from an equidistant spacing defined for $b_{n=1}$ [34]. In Eq. (2), v_g is the group velocity in the bulk material at the pump laser frequency and β_n is the nth-order dispersion coefficient as usually defined in optical materials.

The stability analysis of the equilibrium intracavity field ψ_e of Eq. (1) fulfills the following third-order polynomial:

$$F^2 = \rho^3 - 2\alpha\rho^2 + (\alpha^2 + 1)\rho, \quad (3)$$

with $\rho = |\psi_e|^2$ being the homogeneous steady-state solution. For lower values of the detuning $\alpha < \sqrt{3}$, Eq. (3) has only one single stable real solution. For large detuning $\alpha > \sqrt{3}$, three real-valued solutions ρ_d, ρ_m, and ρ_u might exist, satisfying $\rho_d < \rho_m < \rho_u$, with ρ_d and ρ_u being stable, whereas ρ_m is unstable. The subscripts d, m, and u mean down, middle, and upper, respectively. In the $(\rho - F^2)$ plane, F^2 presents a critical pump power, which is the average of the two extrema [48], following

$$F_c = \sqrt{\frac{2\alpha(\alpha^2 + 9)}{27}}. \quad (4)$$

It is also known that for a pump value lower than F_c, the down steady state ρ_d is favored, while the upper steady state ρ_u is favored instead when the pump applied to the resonator is larger than this critical value [48]. The GVD, TOD, and fourth-order dispersion (FOD) parameters respectively correspond to b_2, b_3, and b_4. By convention, the anomalous GVD regime is defined by $b_2 < 0$, while normal GVD corresponds to $b_2 > 0$. In the next sections, we will investigate the effect of these dispersion parameters on the spatiotemporal dynamics of the cavity, and three main cases will be outlined as a function of the GVD.

3. COEXISTENCE OF SOLITONS WITH ONLY THE TOD

In this section, Eq. (1) is considered with all the dispersion coefficients being equal to zero, except the TOD coefficient b_3 ($b_3 \neq 0$ and $b_{n\neq 3} = 0$). The effect of TOD on dissipative structures has already been analyzed in several research works. Several phenomena have been thereby investigated, such as soliton drift, shift, and (des)tabilization [33,49–54]. In this configuration, bright and dark solitons yielding Kerr combs with single-FSR spacing are obtained (see Fig. 1).

It can also be noted in Fig. 1 that both bright and dark solitons can be obtained depending on the initial condition. As suggested in [36–38], the appropriate way to understand why both bright and dark solitons coexist consists of analyzing the switching waves (SWs) connecting the homogeneous steady-state solutions ρ_d and ρ_u. Their analysis requires that the time derivative must be set to zero. By doing so and by introducing the following intermediate variables $f_{r,i} = \partial_\theta \psi_{r,i}$ and $g_{r,i} = \partial_\theta f_{r,i}$, the LLE (with $b_{n\neq 3} = 0$) can be transformed into a set of first-order differential equations:

$$\partial_\tau \psi_r = f_r, \quad (5)$$

$$\partial_\tau f_r = g_r, \quad (6)$$

$$\partial_\tau g_r = 6\left[\psi_r - \alpha\psi_i - v f_r + \psi_i\psi_r^2 + \psi_i^3 - F\right]/b_3, \quad (7)$$

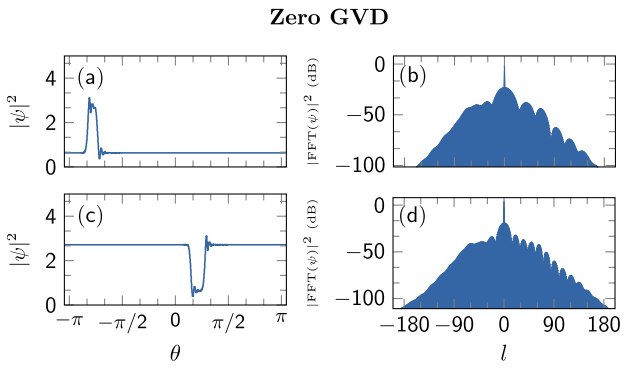

Fig. 1. Coexistence of bright and dark solitons and their corresponding spectra in a zero-GVD regime. The parameters are $\alpha = 2.5$, $b_2 = 0$, $b_3 = 4.08 \times 10^{-5}$ (corresponding to $\beta_3 = 1\ \text{ps}^3/\text{km}$), and $b_4 = 0$. The pump value is $F = \sqrt{6.26} \simeq 1.688$ for both solitons and spectra.

$$\partial_\tau \psi_i = f_i, \tag{8}$$

$$\partial_\tau f_i = g_i, \tag{9}$$

$$\partial_\tau g_r = 6\left[\alpha\psi_r + \psi_i - v f_i - \psi_r \psi_i^2 - \psi_r^3\right]/b_3, \tag{10}$$

where ψ has been expanded into its real ψ_r and imaginary ψ_i parts following $\psi = \psi_r + i\psi_i$ (with $i^2 = -1$). It is important to note that Eq. (1) has been rescaled with regard to $\tau \equiv \theta - vt$, where v is the drift velocity. The spatial eigenvalues of the Jacobian matrix calculated from Eqs. (5)–(10) obey the characteristic equation

$$\lambda^6 + \frac{12v}{b_3}\lambda^4 - \frac{12}{b_3}\lambda^3 + \left(\frac{6v}{b_3}\right)^2\lambda^2 + \frac{36}{b_3^2}\left[1 + \alpha^2 - 4\alpha\rho + 3\rho^2\right] = 0. \tag{11}$$

For being of sixth-order polynomial, Eq. (11) will yield complex value solutions under the form $\lambda = q + i\Omega$, where q is the damping rate and Ω the frequency of the oscillatory tails around ρ_d and ρ_u.

According to [36–38], ρ_d is approached and left by SW_d and SW_u, respectively, which expressions can be linearly approximated by $SW_d \approx \rho_d e^{\lambda_d \theta}$. Similarly, ρ_u is also approached and left by SW_u and SW_d, respectively, which in this case yields $SW_u \approx \rho_u e^{\lambda_u \theta}$. The switching waves and their corresponding spatial eigenvalues are plotted in Fig. 2. As can be seen, the spatial eigenvalues are not symmetric with regard to the oblique gray lines of Figs. 2(b) and 2(d). Therefore, ρ_d and ρ_u are always approached and left in different ways. Moreover, the spatial eigenvalues are complex valued. As a consequence, ρ_d and ρ_u are always approached in an oscillatory way ($\Omega \neq 0$); however, they can be left in a monotonic way (if $\Omega = 0$) or in an oscillatory way. The fact that $\Omega \neq 0$ induces damped oscillations around the steady states. These oscillations occurring on the upper (top) steady state (ρ_u) favors the formation of bright solitons, whereas damping oscillations on the lower (bottom) steady state (ρ_d) are favorable to the formation of dark solitons. These solitons are the consequences of the locking phenomenon of these damping oscillations on each steady state. Therefore, for the same values of the system parameters α, b_3, and F, the lower and the upper steady states ρ_d and ρ_u simultaneously display damped oscillations [see Figs. 2 (a) and 2(c)], so that both bright and dark solitons are susceptible to coexist. Figure 1 evidences the coexistence of these solitons [see Figs. 1(a) and 1(c)] as well as their corresponding frequency combs [see Figs. 1(b) and 1(d)]. It is noteworthy that for an appropriate choice of α, such coexistence of solitons is observed in a narrow region located around the critical pump F_c as was also found in Ref. [48].

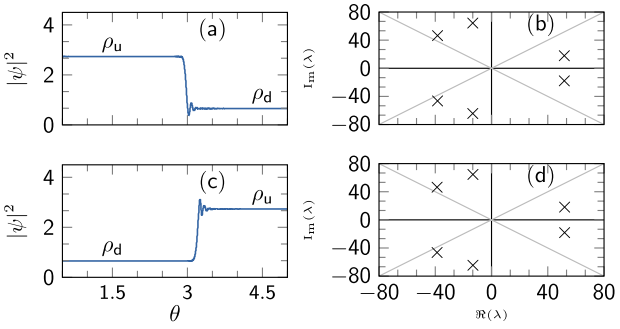

Fig. 2. Switching waves (a) SW_d and (c) SW_u, and the spatial eigenvalues corresponding to λ_d and λ_u are shown in (b) and (d), respectively. λ_d and λ_u are the different solutions of Eq. (11) when $\rho = \rho_d$ and $\rho = \rho_u$, respectively. The oblique gray lines of (b) and (c) materialize the line of symmetric eigenvalues. The parameters are $\alpha = 2.5$, $b_3 = 4.08 \times 10^{-5}$, and $F = \sqrt{2.833} \approx 1.683$.

The next section is devoted to a similar analysis when the GVD is taken into account.

4. COEXISTENCE OF SOLITONS IN NORMAL AND ANOMALOUS GVD

In this section, the effects of normal GVD and anomalous GVD are analyzed separately. Figure 3 evidences the coexistence of both bright and dark solitons (left columns) as well as the single-FSR character of their frequency combs (right columns).

Conserving the value of TOD as in Section 3, and considering normal GVD ($b_2 > 0$), solitons are quenched for the same value of the detuning. However, solitons and their frequency combs are effectively generated if the detuning is increased [in Figs. 3(a)–3(d), $\alpha = 4$ instead of $\alpha = 2.5$ as was the case in Fig. 1]. This result confirms the prediction of [36], according to which for normal GVD, solitons occur only for high values of the detuning. As illustrated in the previous section, these solitons are also originating from the locking of damped oscillations related to the switching waves ($SW_{u,d}$) towards the upper and the lower steady states ρ_d and ρ_u [see Figs. 4(a) and 4(c)]. Applying a similar procedure as in Section 3, the spatial eigenvalues here are solutions of the following sixth-order algebraic polynomial equation:

$$\lambda^6 + \frac{1}{b_3^2}\left(9b_2^2 + 12vb_3\right)\lambda^4 - \frac{12}{b_3}\lambda^3 + \frac{36b_2}{b_3^2}\left(\alpha - 2\rho + \frac{v^2}{b_2}\right)\lambda^2 - \frac{72v}{b_3^2}\lambda + \frac{36}{b_3^2}\left[1 + \alpha^2 - 4\alpha\rho + 3\rho^2\right] = 0, \tag{12}$$

which has nonsymmetric complex-valued solutions [Figs. 4(b) and 4(d)]. Therefore, SW_d and SW_u can develop damped oscillations around ρ_d and ρ_u, which allow bright and dark solitons to form simultaneously. The oscillations of SW_d and SW_u are shown in Figs. 4(a) and 4(c). Like in the case of zero GVD, we obtain the coexistence of both types of solitons around $F = 2.502$, which is close to the critical pump ($F_c \approx 2.72$ for $\alpha = 4$).

When the sign of GVD is negative (anomalous GVD or $b_2 < 0$), bright soliton combs are generated while dark soliton combs are not, even if the detuning is maintained. However, the FOD term can drastically change this situation. This is in accordance with the results of [50], demonstrating that dark solitons can be generated in the anomalous regime only when the FOD dispersion is taken into account. Bright and dark solitons are thereby obtained at high detuning [see Figs. 3(e)–3(h)]. In this case, the oscillations of switching waves, which are responsible

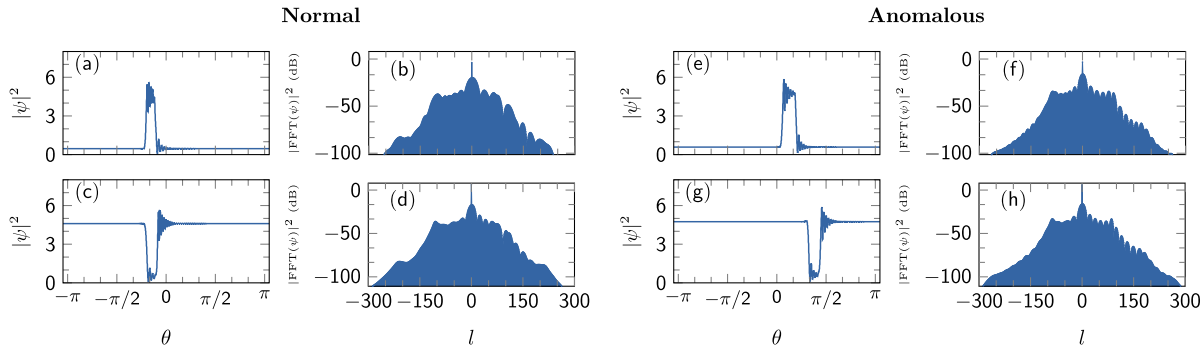

Fig. 3. **Normal**: Coexistence of bright and dark solitons and their corresponding spectra in a normal regime. The parameters are $\alpha = 4$, $b_2 = 4.86 \times 10^{-4}$, $b_3 = 4.08 \times 10^{-5}$, and $b_4 = 0$ (coresponding to $\beta_2 = 1$ ps^2/km and $\beta_3 = 1$ ps^3/km). The pump value is $F = \sqrt{6.26} \approx 2.502$ for both solitons and spectra. **Anomalous**: Coexistence of bright and dark solitons and their corresponding spectra in an anomalous regime. The parameters are $\alpha = 4$, $b_2 = -7.25 \times 10^{-7}$, $b_3 = 4.08 \times 10^{-5}$, $b_4 = 3.93 \times 10^{-10}$ (corresponding to $\beta_2 = -1.45 \times 10^{-3}$ ps^2/km, $\beta_3 = 1$ ps^3/km, and $\beta_4 = 1.15 \times 10^{-4}$ ps^4/km). The FOD is added in order to satisfy the condition required to obtain dark soliton in an anomalous GVD [50]. The pump value is $F = \sqrt{7.41} \approx 2.722$ for both solitons and spectra.

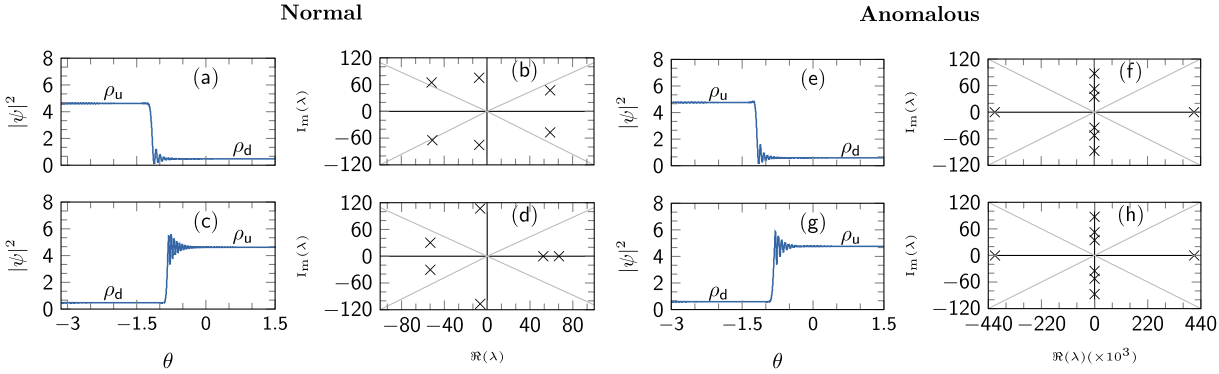

Fig. 4. **Normal**: Switching waves (a) SW$_d$ and (c) SW$_u$, and the spatial eigenvalues corresponding to ρ_d and ρ_u are shown in (b) and (d), respectively. $\alpha = 4$, $b_2 = 4.86 \times 10^{-4}$, $b_3 = 4.08 \times 10^{-5}$, $b_4 = 0$, and $F = \sqrt{6.4} \approx 2.53$. **Anomalous**: Switching waves (e) SW$_d$ and (f) SW$_u$, and the spatial eigenvalues corresponding to ρ_d and ρ_u are shown in (g) and (h), respectively. $\alpha = 4$, $b_2 = -7.25 \times 10^{-7}$, $b_3 = 4.08 \times 10^{-5}$, $b_4 = 3.93 \times 10^{-10}$, and $F = \sqrt{7.5} \approx 2.738$.

for the creation of these solitons, are displayed in Figs. 4(e) and 4(g). As previously demonstrated, these oscillations are the manifestations of the complex and nonsymmetric form of the spatial eigenvalues [see Figs. 4(f) and 4(h)], which are the solution of the following eighth-order polynomial derived from Eq. (1):

$$\lambda^8 - \left(\frac{4b_3}{b_4}\right)^2 \lambda^6 - \frac{96}{b_4^2}\left[\frac{\rho^2(\rho-\alpha)}{F^2} b_4 + \frac{3}{2} b_2^2 + 2b_3 v\right] \lambda^4 + \frac{192 b_3}{b_4^2} \lambda^3 - \frac{576 b_2}{b_4^2}\left[\frac{2\rho^2}{F^2}\left((\rho-\alpha)^2 - 1\right) + \alpha + \frac{v^2}{b_2}\right] \lambda^2 + \frac{1152 v}{b_4^2} \lambda - \frac{576}{b_4^2}\left[1 + \alpha^2 - \frac{4\alpha\rho^2}{F^2}\left((\rho-\alpha)^2 + 1\right)\right] - \frac{1728\rho^4}{F^4 b_4^2}\left((\rho-\alpha)^2 + 1\right)^2 = 0. \tag{13}$$

Once again, like in the case when only the TOD was considered, the coexistence of bright and dark solitons here is also observed in the neighborhood of the critical pump [see Figs. 3(e)–3(h)], that is, around $F_c \approx 2.72$ and calculated from Eq. (4).

In general in this section, we have noticed that for both cases of normal and anomalous GVD, and for a given value of detuning, the widths of solitons are larger when the pump is approaching the critical pump F_c than when it is moving away from F_c. Moreover, a larger pump on the right hand of F_c induces upper steady state ρ_u, while a lower pump far away from F_c leads to the lower steady state ρ_d. Similar results were obtained for the case of zero TOD [48].

5. CONCLUSION

In this work, we have investigated the dynamics of Kerr optical frequency combs when the group-velocity dispersion is positive, negative, or null. All the dispersion parameters have been selected to be relatively small. We have demonstrated that each of these regimes of the group-velocity dispersion enables the emergence of bright and dark solitons. The solitons have also been shown to coexist in specific ranges of the laser pump power and detuning frequency. The formalism of oscillation locking

for switching waves has permitted us to understand how such a phenomenon happens. Future work will focus on the study of the influence of other nonlinear and thermal effects on soliton dynamics [55–57].

Disclosures. The authors declare that there are no conflicts of interest related to this paper.

REFERENCES

1. Y. K. Chembo, "Kerr optical frequency combs: theory, applications and perspectives," Nanophotonics **5**, 214–230 (2016).
2. A. Pasquazi, M. Peccianti, L. Razzari, D. Moss, S. Coen, M. Erkintalo, Y. K. Chembo, T. Hansson, S. Wabnitz, P. Del'Haye, X. Xue, A. M. Weiner, and R. Morandotti, "Micro-combs: a novel generation of optical sources," Phys. Rep. **729**, 1–81 (2018).
3. L. A. Lugiato and R. Lefever, "Spatial dissipative structures in passive optical systems," Phys. Rev. Lett. **58**, 2209 (1987).
4. A. J. Scroggie, W. J. Firth, G. S. McDonalds, M. Tlidi, R. Lefever, and L. A. Lugiato, "Pattern formation in a passive Kerr cavity," Chaos Soliton Fractals **4**, 1323–1354 (1994).
5. L. A. Lugiato, F. Prati, M. L. Gorodetsky, and T. J. Kippenberg, "From the Lugiato–Lefever equation to microresonator-based soliton Kerr frequency combs," Phil. Trans. R. Soc. A **376**, 20180113 (2018).
6. G. Moille, X. Lu, A. Rao, Q. Li, D. A. Westly, L. Ranzani, S. B. Papp, M. Soltani, and K. Srinivasan, "Kerr-microresonator soliton frequency combs at cryogenic temperatures," Phys. Rev. Appl. **12**, 034057 (2019).
7. T. J. Kippenberg, R. Holzwarth, and S. A. Diddams, "Microresonator-based optical frequency combs," Science **332**, 555–559 (2011).
8. D. V. Strekalov, C. Marquardt, A. B. Matsko, H. G. Schwefel, and G. Leuchs, "Nonlinear and quantum optics with whispering gallery resonators," J. Opt. **18**, 123002 (2016).
9. G. Lin, A. Coillet, and Y. K. Chembo, "Nonlinear photonics with high-Q whispering-gallery-mode resonators," Adv. Opt. Photon. **9**, 828–890 (2017).
10. G. Lin and Y. K. Chembo, "Monolithic total internal reflection resonators for applications in photonics," Opt. Mater. X **2**, 100017 (2019).
11. A. B. Matsko, A. A. Savchenkov, W. Liang, V. S. Ilchenko, D. Seidel, and L. Maleki, "Mode-locked Kerr frequency combs," Opt. Lett. **36**, 2845–2847 (2011).
12. Y. K. Chembo and C. R. Menyuk, "Spatiotemporal Lugiato-Lefever formalism for Kerr-comb generation in whispering-gallery-mode resonators," Phys. Rev. A **87**, 053852 (2013).
13. S. Coen, H. G. Randle, T. Sylvestre, and M. Erkintalo, "Modeling of octave-spanning Kerr frequency combs using a generalized mean-field Lugiato–Lefever model," Opt. Lett. **38**, 37–39 (2013).
14. A. Coillet, R. Henriet, K.-P. Huy, M. Jacquot, L. Furfaro, I. Balakireva, L. Larger, and Y. K. Chembo, "Microwave photonics systems based on whispering-gallery-mode resonators," J. Vis. Exp. **78**, e50423 (2013).
15. C. Godey, I. V. Balakireva, A. Coillet, and Y. K. Chembo, "Stability analysis of the spatiotemporal Lugiato-Lefever model for Kerr optical frequency combs in the anomalous and normal dispersion regimes," Phys. Rev. A **89**, 063814 (2014).
16. Y. K. Chembo, "Quantum dynamics of Kerr optical frequency combs below and above threshold: Spontaneous four-wave mixing, entanglement, and squeezed states of light," Phys. Rev. A **93**, 033820 (2016).
17. K. Saleh and Y. K. Chembo, "On the phase noise performance of microwave and millimeter-wave signals generated with versatile Kerr optical frequency combs," Opt. Express **24**, 25043–25056 (2016).
18. P. Del'Haye, A. Schliesser, A. Arcizet, R. Holzwarth, and T. J. Kippenberg, "Optical frequency comb generation from a monolithic microresonator," Nature **450**, 1214–1217 (2007).
19. J. S. Levy, A. Gondarenko, M. A. Foster, A. C. Turner-Foster, A. L. Gaeta, and M. Lipson, "CMOS-compatible multiple-wavelength oscillator for on-chip optical interconnects," Nat. Photonics **4**, 37–40 (2010).
20. F. Ferdous, H. Miao, D. E. Leaird, K. Srinivasan, J. Wang, L. Chen, L. T. Varghese, and A. M. Weiner, "Spectral line-by-line pulse shaping of on-chip microresonator frequency combs," Nat. Photonics **5**, 770–776 (2011).
21. R. D. D. Bitha and A. M. Dikandé, "Elliptic-type soliton combs in optical ring microresonators," Phys. Rev. A **97**, 033813 (2018).
22. N. Picqué, "Frequency comb spectroscopy," Nat. Photonics **13**, 146–157 (2019).
23. Q.-F. Yang, B. Shen, H. Wang, M. Tran, Z. Zhang, K. Y. Yang, L. Wu, C. Bao, J. Bowers, A. Yariv, and K. Vahala, "Vernier spectrometer using counter propagating soliton microcombs," Science **363**, 965–968 (2019).
24. Z. L. Newman, V. Maurice, T. Drake, J. R. Stone, T. C. Briles, D. T. Spencer, C. Fredrick, Q. Li, D. Westly, B. R. Ilic, B. Shen, M.-G. Suh, K. Y. Yang, C. Johnson, D. M. S. Johnson, L. Hollberg, K. J. Vahala, K. Srinivasan, S. A. Diddams, J. Kitching, S. B. Papp, and M. T. Hummon, "Architecture for the photonic integration of an optical atomic clock," Optica **6**, 680–685 (2019).
25. P. Trocha, M. Karpov, D. Ganin, M. H. P. Pfeiffer, A. Kordts, S. Wolf, J. Krockenberger, P. Marin-Palomo, C. Weimann, S. Randel, W. Freude, T. J. Kippenberg, and C. Koos, "Ultrafast optical ranging using microresonator soliton frequency combs," Science **359**, 887–891 (2018).
26. J. Pfeifle, V. Brasch, M. Lauermann, Y. Yu, D. Wegner, T. Herr, K. Hartinger, P. Schindler, J. Li, D. Hillerkuss, R. Schmogrow, C. Weimann, R. Holzwarth, W. Freude, J. Leuthold, T. J. Kippenberg, and C. Koos, "Coherent terabit communications with microresonator Kerr frequency combs," Nat. Photonics **8**, 375–380 (2014).
27. X. Xue, P.-H. Wang, Y. Xuan, M. Qi, and A. M. Weiner, "Microresonator Kerr frequency combs with high conversion efficiency," Laser Photon. Rev. **11**, 1600276 (2017).
28. E. Obrzud, M. Rainer, A. Harutyunyan, M. H. Anderson, J. Liu, M. Geiselmann, B. Chazelas, S. Kundermann, S. Lecomte, M. Cecconi, A. Ghedina, E. Molinari, F. Pepe, F. Wildi, F. Bouchy, T. J. Kippenberg, and T. Herr, "A microphotonic astrocomb," Nat. Photonics **13**, 31–35 (2019).
29. M. Karpov, M. H. P. Pfeiffer, J. Liu, A. Lukashchuk, and T. J. Kippenberg, "Photonic chip-based soliton frequency combs covering the biological imaging window," Nat. Commun. **9**, 1146 (2018).
30. X. Xu, M. Tan, J. Wu, T. G. Nguyen, S. T. Chu, B. E. Little, R. Morandotti, A. Mitchell, and D. J. Moss, "High performance RF filters via bandwidth scaling with Kerr micro-combs," APL Photon. **4**, 026102 (2019).
31. X. Xu, J. Wu, T. G. Nguyen, M. Shoeiby, S. T. Chu, B. E. Little, R. Morandotti, A. Mitchell, and D. J. Moss, "Advanced RF and microwave functions based on an integrated optical frequency comb source," Opt. Express **26**, 2569–2583 (2018).
32. A. L. Gaeta, M. Lipson, and T. J. Kippenberg, "Photonic-chip-based frequency combs," Nat. Photonics **13**, 158–169 (2019).
33. C. Milian and D. V. Skryabin, "Soliton families and resonant radiation in a micro-ring resonator near zero group-velocity dispersion," Opt. Express **22**, 3732–3739 (2014).
34. T. Herr, V. Brasch, J. D. Jost, C. Y. Wang, N. M. Kondratiev, M. L. Gorodetsky, and T. J. Kippenberg, "Temporal solitons in optical microresonators," Nat. Photonics **8**, 145–152 (2014).
35. P. Parra-Rivas, D. Gomila, M. A. Matias, S. Coen, and L. Gelens, "Dynamics of localized and patterned structures in the Lugiato-Lefever equation determine the stability and shape of optical frequency combs," Phys. Rev. A **89**, 043813 (2014).
36. P. Parra-Rivas, D. Gomila, E. Knobloch, S. Coen, and L. Gelens, "Origin and stability of dark pulse Kerr combs in normal dispersion resonators," Opt. Lett. **41**, 2402–2405 (2016).
37. P. Parra-Rivas, E. Knobloch, D. Gomila, and L. Gelens, "Dark solitons in the Lugiato-Lefever equation with normal dispersion," Phys. Rev. A **93**, 063839 (2016).
38. P. Parra-Rivas, D. Gomila, and L. Gelens, "Coexistence of stable dark- and bright-soliton Kerr combs in normal-dispersion resonators," Phys. Rev. A **95**, 053863 (2017).
39. I. S. Grudinin, L. Baumgartel, and N. Yu, "Frequency comb from a microresonator with engineered spectrum," Opt. Express **20**, 6604–6609 (2012).

40. L. Zhang, C. Bao, V. Singh, J. Mu, C. Yang, A. M. Agarwal, L. C. Kimerling, and J. Michel, "Generation of two-cycle pulses and octave-spanning frequency combs in a dispersion-flattened micro-resonator," Opt. Lett. **38**, 5122–5125 (2013).
41. L. Zhang, J. Mu, V. Singh, A. M. Agarwal, L. C. Kimerling, and J. Michel, "Intra-cavity dispersion of microresonators and its engineering for octave-spanning Kerr frequency comb generation," IEEE J. Sel. Top. Quantum Electron. **20**, 111–117 (2014).
42. S. Wang, H. Guo, X. Bai, and X. Zeng, "Broadband Kerr frequency combs and intracavity soliton dynamics influenced by high-order cavity dispersion," Opt. Lett. **39**, 2880–2883 (2014).
43. C. Bao and C. Yang, "Stretched cavity soliton in dispersion-managed Kerr resonators," Phys. Rev. A **92**, 023802 (2015).
44. I. S. Grudinin and N. Yu, "Dispersion engineering of crystalline resonators via microstructuring," Optica **2**, 221–224 (2015).
45. H. M. Mbonde, H. C. Frankis, and J. D. B. Bradley, "Enhanced nonlinearity and engineered anomalous dispersion in coated waveguides," IEEE Photon. J. **12**, 2200210 (2020).
46. N. N. Rozanov, V. E. Semenov, and G. V. Khodova, "Transverse structure of a field in nonlinear bistable interferometers. I. Switching waves and steady-state profiles," Sov. J. Quantum Electron. **12**, 193–197 (1982).
47. S. Coen, M. Tlidi, P. Emplit, and M. Haelterman, "Dynamics of localized and patterned structures in the Lugiato-Lefever equation determine the stability and shape of optical frequency combs," Phys. Rev. Lett. **83**, 2328 (1999).
48. J. H. Talla Mbé, C. Milian, and Y. K. Chembo, "Existence and switching behavior of bright and dark Kerr solitons in whispering-gallery mode resonators with zero group-velocity dispersion," Eur. Phys. J. D **71**, 196 (2017).
49. M. Tlidi, A. Mussot, E. Louvergneaux, G. Kozyreff, A. G. Vladimirov, and M. Taki, "Control and removal of modulational instabilities in low-dispersion photonic crystal fiber cavities," Opt. Lett. **32**, 662–664 (2007).
50. M. Tlidi and L. Gelens, "High-order dispersion stabilizes dark dissipative solitons in all-fiber cavities," Opt. Lett. **35**, 306–308 (2010).
51. M. Taki, A. Mussot, A. Kudlinski, E. Louvergneaux, M. Kolobov, and M. Douay, "Third-order dispersion for generating optical rogue solitons," Phys. Lett. A. **374**, 691–695 (2010).
52. M. Tlidi, L. Cherbi, A. Hariz, and S. Coulibaly, "Drift of dark cavity solitons in a photonic-crystal fiber resonator," Phys. Rev. A. **88**, 035802 (2013).
53. P. Parra-Rivas, D. Gomila, F. Leo, S. Coen, and L. Gelens, "Third-order chromatic dispersion stabilizes Kerr frequency combs," Opt. Lett. **39**, 2971–2974 (2014).
54. F. Leo, S. Coen, P. Kockaert, P. Emplit, M. Haelterman, A. Mussot, and M. Taki, "Impact of third-order dispersion on nonlinear bifurcations in optical resonators," Phys. Lett. A. **379**, 1934–1937 (2015).
55. G. Lin and Y. K. Chembo, "Phase-locking transition in Raman combs generated with whispering gallery mode resonators," Opt. Lett. **41**, 3718–3721 (2016).
56. G. Lin, S. Diallo, J. Dudley, and Y. K. Chembo, "Universal nonlinear scattering in ultra-high Q whispering gallery-mode resonators," Opt. Express **24**, 14880–14894 (2016).
57. S. Diallo, G. Lin, and Y. K. Chembo, "Giant thermo-optical relaxation oscillations in millimeter-size whispering gallery mode disk resonators," Opt. Lett. **40**, 3834–3837 (2015).